

University of Nebraska - Lincoln

DigitalCommons@University of Nebraska - Lincoln

---

Mechanical & Materials Engineering Faculty  
Publications

Mechanical & Materials Engineering, Department  
of

---

2014

# Measurement of hydrodynamic force generation by swimming dolphins using bubble DPIV

Frank E. Fish

*West Chester University, ffish@wcupa.edu*

Paul Legac

*Rensselaer Polytechnic Institute, Troy*


Terrie M. Williams

*University of California, Santa Cruz*

Timothy Wei

*University of Nebraska-Lincoln, twei3@unl.edu*

Follow this and additional works at: <http://digitalcommons.unl.edu/mechengfacpub>

 Part of the [Mechanics of Materials Commons](#), [Nanoscience and Nanotechnology Commons](#), [Other Engineering Science and Materials Commons](#), and the [Other Mechanical Engineering Commons](#)

---

Fish, Frank E.; Legac, Paul; Williams, Terrie M.; and Wei, Timothy, "Measurement of hydrodynamic force generation by swimming dolphins using bubble DPIV" (2014). *Mechanical & Materials Engineering Faculty Publications*. 150.  
<http://digitalcommons.unl.edu/mechengfacpub/150>

This Article is brought to you for free and open access by the Mechanical & Materials Engineering, Department of at DigitalCommons@University of Nebraska - Lincoln. It has been accepted for inclusion in Mechanical & Materials Engineering Faculty Publications by an authorized administrator of DigitalCommons@University of Nebraska - Lincoln.

## RESEARCH ARTICLE

# Measurement of hydrodynamic force generation by swimming dolphins using bubble DPIV

 Frank E. Fish<sup>1,\*</sup>, Paul Legac<sup>2</sup>, Terrie M. Williams<sup>3</sup> and Timothy Wei<sup>4</sup>
**ABSTRACT**

Attempts to measure the propulsive forces produced by swimming dolphins have been limited. Previous uses of computational hydrodynamic models and gliding experiments have provided estimates of thrust production by dolphins, but these were indirect tests that relied on various assumptions. The thrust produced by two actively swimming bottlenose dolphins (*Tursiops truncatus*) was directly measured using digital particle image velocimetry (DPIV). For dolphins swimming in a large outdoor pool, the DPIV method used illuminated microbubbles that were generated in a narrow sheet from a finely porous hose and a compressed air source. The movement of the bubbles was tracked with a high-speed video camera. Dolphins swam at speeds of 0.7 to 3.4 m s<sup>-1</sup> within the bubble sheet oriented along the midsagittal plane of the animal. The wake of the dolphin was visualized as the microbubbles were displaced because of the action of the propulsive flukes and jet flow. The oscillations of the dolphin flukes were shown to generate strong vortices in the wake. Thrust production was measured from the vortex strength through the Kutta–Joukowski theorem of aerodynamics. The dolphins generated up to 700 N during small amplitude swimming and up to 1468 N during large amplitude starts. The results of this study demonstrated that bubble DPIV can be used effectively to measure the thrust produced by large-bodied dolphins.

**KEY WORDS:** Dolphin, Hydrodynamics, Bubble DPIV, *Tursiops truncatus*, Swimming, Gray's paradox

**INTRODUCTION**

It has been a longstanding impression both within as well as outside of the scientific community that dolphins swim with a low energy expenditure (Fish and Hui, 1991; Fish and Rohr, 1999). As movement through water is difficult because of the higher density and viscosity of the medium compared with air (Denny, 1993; Vogel, 1994), the mechanics of high-speed swimming by dolphins has been of considerable interest (Gray, 1936; Lang and Daybell, 1963; Lang, 1975; Aleyev, 1977; Fish and Hui, 1991; Williams et al., 1992; Fish and Rohr, 1999; Nagai, 1999; Romanenko, 2002; Fish, 2006). Studies on dolphin swimming have thus focused on the development of muscular power output and enhanced mechanisms of thrust production, or special drag reduction mechanisms.

Swimming encompasses the transfer of kinetic energy and momentum from the animal's propulsive movements to the water.

A dolphin swimming at constant speed balances forces and moments acting on it by the principle of momentum conservation. The total thrust produced by the action of the caudal flukes balances the total resistance (i.e. drag) that the animal's body encounters moving forward (Webb, 1975; Sfakiotakis et al., 1999; Schultz and Webb, 2002). By directly measuring the flow generated by fluke oscillations, the thrust, which is indistinguishable from the drag (Schultz and Webb, 2002), for a steadily swimming dolphin can be computed. The momentum imparted to water by an oscillating hydrofoil is visualized in a thrust-type (reverse von Kármán street) wake as a central momentum jet flow, which is directed through the center of a staggered array of vortex rings (Weihs, 1972; Skrovan et al., 1999; Fish and Lauder, 2006).

The challenge to date has been the inability either to directly measure the thrust generated by a swimming dolphin or to measure the associated flow field. Here we solve this problem for the first time and describe the thrust produced by an actively swimming dolphin using digital particle image velocimetry (DPIV). DPIV is a video-based flow measurement technique first introduced and named by Willert and Gharib (Willert and Gharib, 1991). It is a variant of the film-based technique, particle image velocimetry (PIV) or pulsed laser velocimetry, developed a decade earlier (Adrian, 1984; Adrian and Yao, 1985). The basic concept of DPIV is that images of very small, neutrally buoyant particles that are small enough to follow fluid motions, but large enough to be imaged by the camera, are statistically tracked from one video frame to the next (Willert and Gharib, 1991). The seeded flow is typically illuminated by light from a pulsed laser, which is synchronized to the video framing rate with one laser pulse occurring in each video frame. The time between laser pulses is set small enough that particle displacements from one video frame to the next are limited to a few pixels. The particle displacements divided by the time between successive video frames yields temporally and spatially resolved flow velocity field information. The video sequence is then digitized and used as input to a DPIV processing program.

Since Willert and Gharib's (Willert and Gharib, 1991) seminal work, more sophisticated correlation algorithms have been developed to improve both accuracy and resolution of the technique. A multiple correlation algorithm was developed in-house to resolve accuracy, resolution and reliability limitations not present in other packages at that time (Grega et al., 1995; Hsu et al., 2000). Further development work permitting measurement of fluid acceleration is described in Dong et al. (Dong et al., 2001).

The use of DPIV as an experimental technique allows visualization of the wake and near-body flow patterns to quantify flow velocities, momentum changes and magnitudes of propulsive forces for swimming animals (Müller et al., 1997; Drucker and Lauder, 1999; Drucker and Lauder, 2001; Lauder et al., 2002; Schultz and Webb, 2002). Laboratory experiments using DPIV were conducted using laser sheets to illuminate ~10 µm diameter silver-coated glass beads in the wake of the fish (Fish and Lauder, 2006;

<sup>1</sup>Department of Biology, West Chester University, West Chester, PA 19383, USA.

<sup>2</sup>Department of Mechanical, Aerospace and Nuclear Engineering, Rensselaer Polytechnic Institute, Troy, NY 12180, USA. <sup>3</sup>Center for Ocean Health, Long Marine Laboratory, University of California, Santa Cruz, Santa Cruz, CA 95060, USA.

<sup>4</sup>College of Engineering, University of Nebraska, Lincoln, NE 68588, USA.

\*Author for correspondence (ffish@wcupa.edu)

Received 7 March 2013; Accepted 19 September 2013

**List of symbols and abbreviations**

$A$	surface area
AR	aspect ratio
$b$	fluke span
$C_D$	coefficient of drag
DPIV	digital particle image velocimetry
$ds$	differential tangent vectors
$L$	body length
PIV	particle image velocimetry
$Re$	Reynolds number
$T$	thrust
$\nu$	kinematic viscosity
$\mathbf{V}$	velocity around the vortex contour
$V_{swim}$	swimming velocity
$V_{tail}$	vertical velocity of the tail
$\Gamma$	vortex circulation
$\rho$	fluid density

Flammang et al., 2011). Based on the movement of the glass beads, velocity data were used to quantify the thrust-producing momentum jet and vortices.

The size of a dolphin, its protected status and the volume of water needed to permit continuous swimming preclude use of the standard DPIV setup. Specifically, modifications to the DPIV technique are necessary to accommodate health and safety issues for dolphins, which prevent the use of lasers and biologically hazardous seeding particles. We, therefore, examined the wake structure of bottlenose dolphins [*Tursiops truncatus* Motagu 1821)] using microbubbles (<1 mm) generated in a nominally planar sheet. This technique allowed direct measurements of the wake and propulsive forces from oscillation of the flukes of actively swimming dolphins in order to test long-held hypotheses on thrust production.

**RESULTS**

The dolphins swam at speeds ( $V_{swim}$ ) ranging from 0.6 to 3.7 m s<sup>-1</sup>. For this range of velocities, the corresponding range of Reynolds numbers ( $Re$ ) was  $1.6 \times 10^6$  to  $7.7 \times 10^6$ . The peak-to-peak amplitude

(i.e. vertical displacement of fluke tip over one half cycle) during small amplitude swimming was  $0.30 \pm 0.12$  m and ranged from 0.14 to 0.47 m, which was 5.8–19.4% of body length. This range was below the typical peak-to-peak amplitude of 20% of body length for cetaceans (Fish, 1998a; Rohr and Fish, 2004). The low values may have reflected the generally low swimming speed as the dolphin followed the trainer's target. Frequency of the fluke stroke varied from 0.5 to 2.9 Hz for small amplitude swimming. As the flukes exhibited only half a stroke cycle in the field of view, the frequency was not measured for large amplitude starts. The peak-to-peak amplitude for large amplitude starts was  $0.68 \pm 0.14$  m, which was 2.2 times greater than the mean value for small amplitude swimming. Large stroke amplitudes for *T. truncatus* occur at the start of horizontal swims and the beginning of descent and ascent phases of dives (Skrovan et al., 1999).

The dorsoventral oscillations of the flukes produced pairs of counter-rotating vortices during each propulsive cycle. One vortex was generated for each upstroke and each downstroke of the tail (Figs 1–3). The vortex was shed from the trailing edge of the flukes.

Using Eqn 1 (see Materials and methods), the mean circulation in the vortices generated by the flukes during small amplitude swimming was  $0.184 \pm 0.077$  m<sup>2</sup> s<sup>-1</sup>. The computed thrust varied from 50.8 to 700.4 N for small amplitude swimming and 334.0 to 1467.6 N for large amplitude starts in which the dolphin accelerated rapidly from rest (Fig. 4).

Thrust increased curvilinearly with small amplitude swimming speed (Fig. 4). This trend was consistent with thrust for dolphins calculated from hydrodynamic models (Fish, 1993; Fish, 1998a). For small amplitude swimming by the dolphins in the present study, the relationship between thrust ( $T$ ) and  $V_{swim}$  was described by the regression equation  $T = 112.33 V_{swim}^{1.26}$ , which had a correlation coefficient of 0.83. However, the exponent of 1.26 was below the predicted exponent of 2 (Webb, 1975). This low exponent may have been due to the limited range of swimming speeds of the dolphins. The median swimming speed of the two dolphins was 1.57 m s<sup>-1</sup>. The low swimming speeds in this study were below the speeds associated with minimum cost of transport



**Fig. 1.** Interconnected vortices generated in a microbubble curtain by oscillations of the flukes of a dolphin.

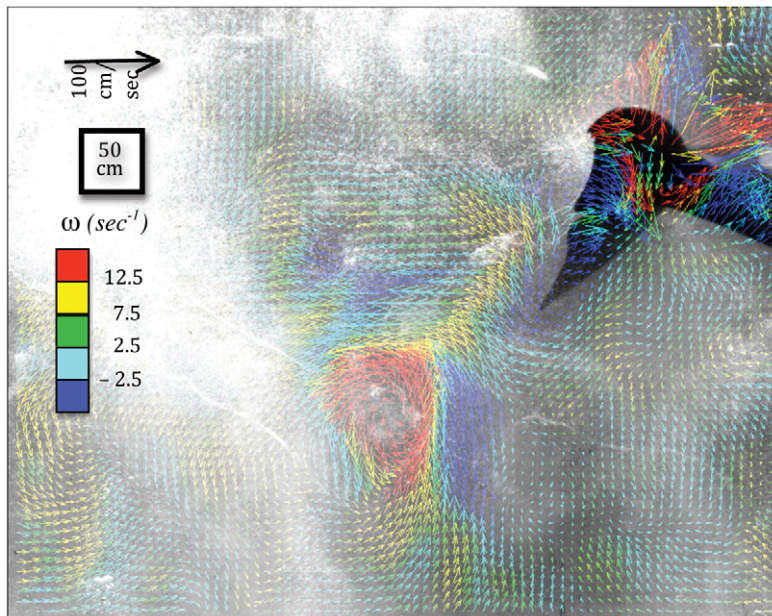


**Fig. 2. Vortex generated by a large amplitude fluke stroke from a swimming dolphin.** Velocity vectors are colored and based on vorticity, and the mean rise of the bubbles has been subtracted. The white box is the control volume used to determine the circulation of the vortex, in this case  $\Gamma=0.19 \text{ m}^2 \text{ s}^{-1}$  and  $T=700 \text{ N}$ . The field of view is 1.2 m wide and 0.95 m high. There are 78 and 62 vectors in the horizontal and vertical directions, respectively. The spacing between vectors is  $\sim 1.56 \text{ cm}$ . Each vector is assigned a color corresponding to the local vorticity or fluid rotation rate,  $\omega$ . Colors indicate the magnitude of  $\omega$ , where red corresponds to positive or counterclockwise rotation ( $\omega \geq 15,000 \text{ s}^{-1}$ ) and blue indicates negative or clockwise rotation. The largest velocity magnitude in the image is  $\sim 67 \text{ cm s}^{-1}$ , located just to the right of the tail vortex center; the maximum vorticity value at the vortex core is  $17,500 \text{ s}^{-1}$ .

for *T. truncatus* of  $2.1 \text{ m s}^{-1}$  (Williams et al., 1993) and  $2.5 \text{ m s}^{-1}$  (Yazdi et al., 1999).

The range of thrust values corresponds to mechanical power outputs of 36.1–549.3 W for small amplitude swimming and up to 5.4 kW for a large amplitude start. This is a 149-fold increase in power for an approximate 5.2-fold increase in speed. As the percentage of adult body mass comprising the locomotor muscles of dolphins is 25.7% (Dearolf et al., 2000), the maximum mass-specific muscle power output is  $0.7\text{--}46.8 \text{ W kg}^{-1}$  for small amplitude swimming with a maximum recorded value of  $100.1 \text{ W kg}^{-1}$  for a large amplitude start. These values are within the range of power outputs for vertebrate muscle (Weis-Fogh and Alexander, 1977; Josephson, 1993).

Thrust calculated from the vortices during small amplitude swimming at  $V_{\text{swim}}$  below  $1.5 \text{ m s}^{-1}$  compared closely with previously reported thrust values for *T. truncatus*, based on calculations from lifting wing theory (Chopra and Kambe, 1977; Fish, 1998a). Above  $1.5 \text{ m s}^{-1}$ , the thrust from the present study increased to a maximum that was approximately 2.7 times higher than the calculated thrust at  $3.4 \text{ m s}^{-1}$ .

For the dolphins accelerating from rest in the horizontal direction to the image capture plane, the circulation of the vortices was on average 1.8 times greater than the circulation produced during small amplitude swimming. This greater circulation during a large amplitude start occurred even though the dolphins had attained similar speeds with small amplitude swimming. The thrust from

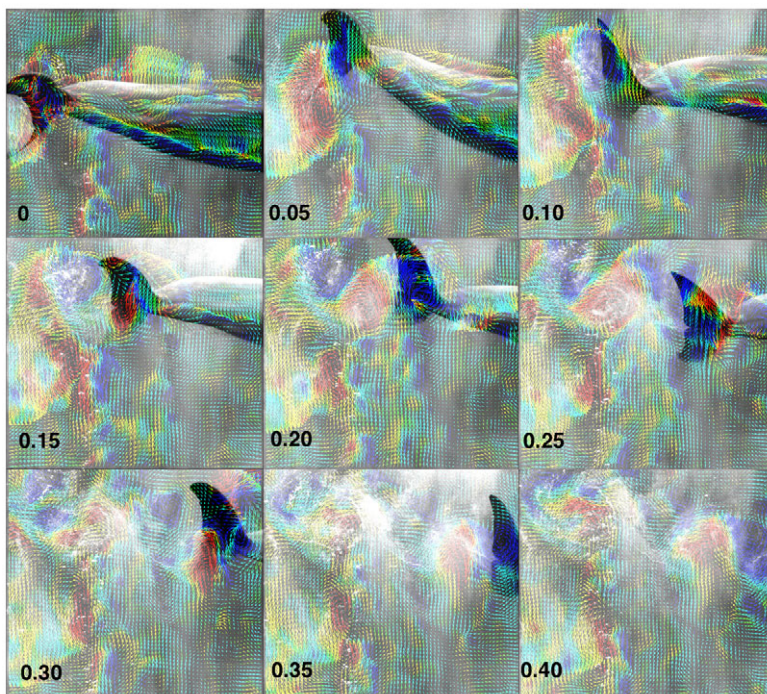


**Fig. 3. Composite photographs of the small amplitude stroke cycle of a swimming dolphin.** Time in seconds for each frame in the sequence is shown in the bottom left of each frame. Velocity vectors are colored and based on vorticity, and the mean rise of the bubbles has been subtracted. Length and color scales are the same as those used in Fig. 2.

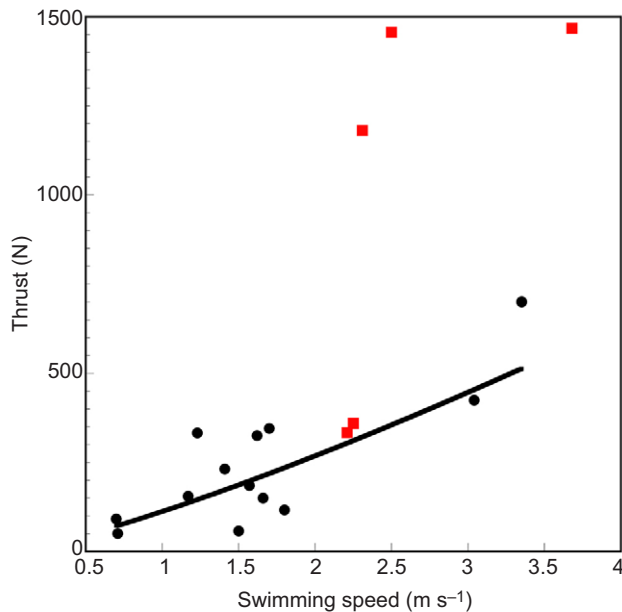


**Fig. 4.** The thrust ( $T$ ) determined from wake vorticity is plotted as a function of swimming velocity for bottlenose dolphins. Black circles are for dolphins that are swimming steadily and red squares are for large amplitude starts. The black line denotes the regression of data.

large amplitude starts was 2.1–2.9 times greater than for small amplitude swimming over similar speeds (Fig. 4).

Computed values of the coefficient of drag ( $C_D$ ) were based on small amplitude swimming only.  $C_D$  for dolphins ranged from 0.009 to 0.016 with a mean of  $0.014 \pm 0.003$ . The relationship between the  $C_D$  data and  $Re$  is described by the equation  $C_D = 16.99Re^{0.47}$ . Values of  $C_D$  for the dolphins were compared with theoretical minimum drag coefficients (Fig. 5). All  $C_D$  values were higher than the theoretical minimum values and occurred in the region of a fully developed turbulent boundary layer. For equivalent  $Re$ ,  $C_D$  values for the dolphins were 19.1–20.0 and 3.2–4.9 times greater than theoretical minimum values for flow over a flat plate with laminar and turbulent boundary layers, respectively.

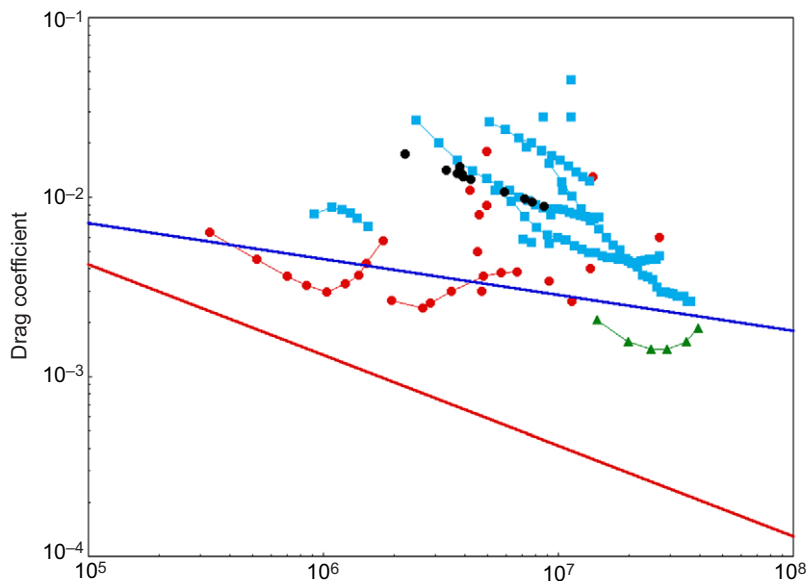


**Fig. 5.** Comparison of drag coefficients plotted against Reynolds number for cetaceans. Data were obtained from experiments on rigid models, towed bodies and gliding animals (blue circles), from hydrodynamic models based on swimming kinematics (red squares), from a rigid 'dolphin' model with the shape of a solid of revolution of the NACA 66 series (green triangles), and from the present study (black circles) (from Lang and Daybell, 1963; Lang and Pryor, 1966; Aleyev and Kurbatov, 1974; Kayan, 1974; Purves et al., 1975; Webb, 1975; Aleyev, 1977; Chopra and Kambe, 1977; Yates, 1983; Videler and Kamermans, 1985; Fish, 1998a). The black line represents the frictional drag coefficient for a flat plate with turbulent boundary layer flow and the red line is for a flat plate with laminar boundary flow.

## DISCUSSION

### Thrust production

The results of bubble DPIV clearly showed a vortex wake that was generated from the pitching and heaving motions of the flukes of the dolphins. The wake velocity and the associated mass of water generated momentum, which is transferred from the action of the flukes to the water. The momentum imparted to the fluid was concentrated in a jet of fluid directed, on average, opposite to the swimming direction (Wu, 1971a; Rayner, 1985; Triantafyllou et al., 1993; Anderson et al., 1998).

Thrust is derived from the reaction of the momentum jet. The jet induces the resting water around it to generate a vortex wake. The vortex wake is arranged as a staggered array of vortices that move downstream from the flukes (Triantafyllou et al., 1991). The vortices are displayed as alternating clockwise and counterclockwise vortex rings in two dimensions, but are connected in three dimensions with the jet directed through the center of the rings (Vogel, 1994). The rotation of the vortices is opposite to the von Kármán street behind stationary objects in a flow, which creates drag (Weihs, 1972; Triantafyllou et al., 1991).

The basis for thrust production by the dolphins is that, as the flukes oscillate, they are pitched at a positive angle of attack to the oncoming flow. The fluid is deflected above and below the flukes imparting a velocity difference between the two surfaces. By the Bernoulli theorem, a net pressure difference results in a force, which is resolved into a drag that is tangent to the axis of the motion of the flukes and a lift that is perpendicular to the axis of motion and canted anteriorly (Webb, 1975). The anteriorly directed lift is resolved into a vector component, which represents the thrust. As thrust from lift is produced, momentum is transferred from the flukes to the water. At a constant swimming speed, the thrust produced balances the viscous and pressure drag of the body and flukes.

Because the flukes are connected to the body by a narrow attachment, the caudal peduncle, which oscillates in the direction of its minimum resistance, the flukes are essentially separated from the body (Lighthill, 1969; Lighthill, 1970; Fish et al., 1988; Fish and Hui, 1991; Fish, 1993; Fish, 1998a). This allowed for analysis of thrust production by the flukes to be made separate from the body and its actions, and the drag produced.

The quantitative measurement of flow using bubble DPIV to determine thrust production was largely instigated by previous

analyses of the energetics of dolphin swimming. In the first such study, Gray (Gray, 1936) calculated the power output of a swimming dolphin by assessing its thrust production, using a simple drag-based model and assumptions of muscle power output. Ultimately, Gray argued that dolphins could not swim at their extraordinary speeds,  $\sim 10 \text{ m s}^{-1}$ , with the available muscle mass unless special hydrodynamic drag-reducing mechanisms were used (i.e. maintenance of a laminar boundary layer). The inconsistency between hydrodynamic power needed to attain high swimming speeds and the available muscle power became known as 'Gray's paradox' (Parry, 1949; Fish, 2006).

Following the resistance model used by Gray (Gray, 1936), Kermack (Kermack, 1948) estimated the power output for the blue whale (*Balaenoptera musculus*) and the fin whale (*Balaenoptera physalus*). Assuming a swimming speed of  $12.9 \text{ m s}^{-1}$  (25 knots) with fully laminar or fully turbulent boundary layer flows, thrust power was calculated as 15.5 and 291.6 kW for the fin whale and 19.5 and 398.9 kW for the blue whale, respectively.

Parry (Parry, 1949) developed a quasi-static resistance model based on fluke motion. He showed schematically how thrust was generated as a resultant of a hydrodynamically derived force. A quasi-steady approach was used by Kayan (Kayan, 1979) based on the lift and drag characteristics of isolated flukes for *Tursiops* and integrated over the entire stroke cycle. Although Kayan (Kayan, 1979) considered the values from his model to represent maxima, results indicated low thrust production (Fish and Rohr, 1999). The quasi-steady approach assumes that the forces acting on the flukes at any instant are the same as those acting under equivalent steady-state conditions of velocity and angle of attack (Webb, 1975). Quasi-steady estimates are not directly translated to thrust production because of the unsteady oscillatory motions of the flukes. Videler and Kamermans (Videler and Kamermans, 1985) were unable to reconcile inertial forces, necessary to accelerate the body and entrained fluid, that were fivefold larger than the propulsive forces calculated with a quasi-steady model.

In cases where  $Re > 10^3$ , there are large inertial effects (Lighthill, 1970; Webb, 1975). Acceleration reactions, associated with imparting momentum to the water, become more important and increase power output (Daniel, 1984; Daniel et al., 1992). Unsteady effects may contribute to thrust production by increasing the relative velocity and thus the lift (Daniel et al., 1992). An additional limitation of the quasi-steady approach is its reliance on the lift characteristics of conventional foil sections in steady flows. Foils similar to whale flukes under steady flow conditions stall at angles of attack over 20 deg (Abbott and von Doenhoff, 1959). However, an oscillating high aspect ratio fin can continue to generate lift, and thus thrust, up to an attack angle of 30 deg (Triantafyllou and Triantafyllou, 1995).

To comprehend the dynamic production of lift-based thrust from high aspect ratio lunate tails, Lighthill (Lighthill, 1969; Lighthill, 1970) suggested the use of unsteady lifting-line theory. Numerical calculations of thrust and propulsive efficiency of oscillating rigid flat plates as a three-dimensional lunate-tail model were made by Chopra and Kambe (Chopra and Kambe, 1977) for a series of swept planforms and by Lan (Lan, 1979) and Liu and Bose (Liu and Bose, 1993) using a quasi-vortex lattice method. The latter method was considered superior, because it could be applied to arbitrary planforms and reliably predicted leading-edge suction (Liu and Bose, 1993). Lan (Lan, 1979) found a 20% lower thrust than Chopra and Kambe (Chopra and Kambe, 1977), although the predicted efficiency was in good agreement (Yates, 1983). Unsteady lifting surface models were applied to the kinematics of thunniform

swimmers (e.g. tuna, phocid seals, cetaceans) (Webb, 1975; Chopra and Kambe, 1977; Yates, 1983; Fish et al., 1988; Fish, 1993; Fish, 1998a; Bose, and Lien, 1989) to calculate the thrust and mechanical power output.

While computational methods provided estimations of thrust production for dolphins that indicate high levels, the flukes have been treated as rigid, flat plates. The flukes have a three-dimensional architecture with a cross-sectional profile that resembles engineered wing sections with a rounded leading edge and a long tapering tail (Lang, 1966; Purves, 1969; Fish, 1998b; Fish et al., 2007; Fontanella et al., 2011). Like the engineered foils, flukes possess a structure that could produce high lift with low drag (Fish et al., 2007). The rounded leading edge promotes a suction force that further contributes to lift (Lighthill, 1970; Wu, 1971b; Chopra and Kambe, 1977). The effect of leading-edge suction is to tilt the pressure force forward by an angle equal to the angle of attack (D. Weihs, pers. comm.). The total lift force, which is typically normal to the fluke axis, is tilted perpendicular to the direction of fluke motion and thus increases the thrust component. Additional thrust would produce a leading-edge vortex, which has been hypothesized for fish-like swimming with a highly sweptback tail (Borazjani and Daghooghi, 2013).

Furthermore, the flukes are flexible (Romanenko, 2002; Fish et al., 2006). Flexibility across the chord and span can increase thrust and propulsive efficiency (Katz and Weihs, 1978; Yamaguchi and Bose, 1994; Bose, 1995; Liu and Bose, 1997). Cambering by bending of the flukes throughout the stroke cycle could provide increased lift with a concomitant increase in thrust (Fish et al., 2006). Therefore, measurements and calculations of lift and drag performance by static, rigid hydrofoils without consideration of flexibility permit only a rudimentary understanding of the development of thrust by oscillating flukes.

### Thrust comparisons among cetaceans

Estimates of thrust power based on different models for a variety of cetacean species are displayed in Fig. 6 and summarized in Table 1. To compensate for differences due to size, the thrust power was divided by body mass. Although slightly higher, the thrust power measurements for dolphins based on bubble DPIV over a range of swimming speeds were in line with values for cetaceans using computational models (Fig. 6). However, the thrust power for small amplitude swimming increased as a power function with swimming speed with an exponent of 2.26, which was 0.64 times smaller than the exponent of 3.53 for thrust power based on other studies. The mass-specific power estimates from bubble DPIV were equivalent to published values (Table 1).

Particular errors are associated with each model employed for cetacean swimming based on the assumptions used (see above). Swimming was assumed to be rectilinear with the exception of Hui (Hui, 1987), who examined dolphins swimming in small circular pools. Hui (Hui, 1987) introduced a correction factor of 4.77–5.24 for the added centripetal energy required for turning.

Gray's (Gray, 1936) original calculations of thrust power (1939 W) for a dolphin with turbulent conditions provided a mass-specific thrust power of  $21.4 \text{ W kg}^{-1}$ . At the time, this value was believed to be too high for the dolphin based on muscle power output (Fish, 2006). However, data from Table 1 show that the thrust power calculated by Gray (Gray, 1936) is low compared with other studies when it is considered that the dolphin was swimming at  $10.1 \text{ m s}^{-1}$ . Gray's drag-based model considered the dolphin to be a rigid body with a drag coefficient based on a theoretical flat plate. Higher power outputs from bubble DPIV and other computational

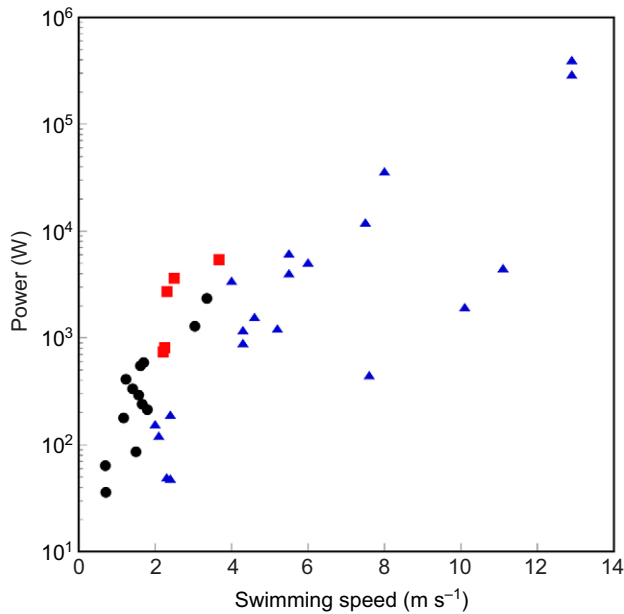


**Fig. 6. Comparison of thrust power measurements for cetaceans over a range of swimming speeds.** Values are displayed from this study using digital particle image velocimetry for small amplitude (solid black circles) and large amplitude (solid red squares) swimming, and from previous studies using computational methods (solid blue triangles) as described in the text (see Thrust comparisons among cetaceans).

models were based on actively swimming dolphins. The effects of propulsive body movements may increase power output by three to five times (Lighthill, 1971; Liu et al., 1997; Anderson et al., 2001). In addition, pressure drag can increase as the animal swims, because

propulsive motions of the body deviate from the streamlined position (Williams and Kooyman, 1985; Fish et al., 1988; Fish, 1993; Fish et al., 2003).

The quasi-steady model appears to give higher values of thrust power compared with other models over a similar range of swimming speeds (Table 1). Webb (Webb, 1975) applied the model developed by Parry (Parry, 1949) to data from Norris and Prescott (Norris and Prescott, 1961) and Lang and Daybell (Lang and Daybell, 1963) for *Delphinus bairdi*, *Phocoenoides dalli* and *Lagenorhynchus obliquidens* swimming at 4.3, 4.3 and 5.54 m s<sup>-1</sup>, respectively. The thrust power developed was 896, 1800 and 6180 W for *D. bairdi*, *P. dalli* and *L. obliquidens*, respectively. These values were 6.3–16.0 times greater than the thrust power based on the theoretical frictional drag power of a flat plate with turbulent boundary conditions. Webb (Webb, 1975) considered that the high thrust power values were the result of increased drag from swimming near the water surface. Drag can increase by up to five times the frictional drag when swimming near the surface (Hertel, 1966).

Fish (Fish, 1998a) found that thrust power was highly dependent on swimming velocity and size. Based on unsteady lifting wing theory (Chopra and Kambe, 1977), the calculated power output showed a curvilinear increase with increasing swimming speed for four cetacean species examined. Maximal performance was explored by Lang and Pryor (Lang and Pryor, 1966) for an accelerating *Stenella attenuata*. At a maximum speed of 11.1 m s<sup>-1</sup>, thrust power was 4517.8 W with a mass-specific thrust power of 85.7 W kg<sup>-1</sup>. This high power output could only be maintained for an acceleration of 1.5 s. Although the dolphin maintained speed, its power output decreased below the maximum power by 30% after the acceleration.

Goforth (Goforth, 1990) developed a technique in which dolphins (*T. truncatus*) were trained to push against a load cell to directly

**Table 1. Estimates of thrust power**

Species	Mass (kg)	Length (m)	$U$ (m s <sup>-1</sup> )	Model	Thrust power (W)	Mass-specific power (W kg <sup>-1</sup> )	Source
<i>Balaenoptera musculus</i>	n.a.	25.9	12.9	D	398,949.5	–	Kermack, 1948
<i>Balaenoptera physalus</i>	n.a.	21.0	12.9	D	291,568.7	–	Kermack, 1948
	27,000	14.5	12.0	US	208,800.0	7.3	Bose and Lien, 1989
<i>Delphinus bairdi</i>	n.a.	1.7	4.3	QS	896.0	–	Webb, 1975
<i>Delphinus delphis</i>	90.7	1.8	10.1	D	1938.8	21.4	Gray, 1936
	59.2	1.7	2.4	D	190.8	3.2	Hui, 1987
	54.7	1.8	2.1	D	122.1	2.2	Hui, 1987
<i>Delphinapterus leucas</i>	664.2	3.6	4.0	US	3436.0	5.2	Fish, 1998a
<i>Lagenorhynchus obliquidens</i>	91.0	2.1	4.6	A	1568.0	17.2	Lang and Daybell, 1963
	91.0	2.1	5.5	QS	6180.0	67.9	Webb, 1975
	91.0	2.1	5.5	US	4030.0	44.3	Webb, 1975
	91.0	2.1	5.2	US	1223.7	13.4	Yates, 1983
<i>Phocoena phocoena</i>	24.0	1.2	7.6	D	447.4	18.6	Gray, 1936
<i>Phocoenoides dalli</i>	n.a.	2.0	4.3	QS	1180.0	–	Webb, 1975
<i>Orcinus orca</i>	1645.4	4.8	8.0	US	36,259.6	22.0	Fish, 1998a
<i>Pseudorca crassidens</i>	535.8	3.8	7.5	US	12,065.7	22.5	Fish, 1998a
<i>Stenella attenuata</i>	52.7	1.9	11.1	A	4517.8	85.7	Lang and Pryor, 1966
<i>Sotalia guianensis</i>	85.0	1.9	2.4	A	48.4	0.6	Videler and Kamermans, 1985
<i>Tursiops truncatus</i>	140.0	2.4	2.3	QS	49.6	0.4	Kayan, 1979
	232.0	2.5	2.0	A	155.5	0.7	Videler and Kamermans, 1985
	214.9	2.6	6.0	US	5090.9	23.7	Fish, 1998a
<i>T. truncatus</i> (small amplitude)	80.8	2.4	3.4	DPIV	2346.3	13.0	Present study
<i>T. truncatus</i> (large amplitude)	210.0	2.5	3.7	DPIV	5393.5	25.7	Present study

Models: A, acceleration (Lang and Daybell, 1963); D, drag-based (Gray, 1936); DPIV, digital particle image velocimetry (present study); QS, quasi-steady (Parry, 1949); US, unsteady lifting surface (Lighthill, 1969; Chopra and Kambe, 1977).

n.a., not available.

measure the force generated by the animal's swimming actions. Dolphins were able to produce maximum forces during static swimming of 1.08–1.56 times body mass and forces of 0.3–0.6 times body mass at maximum oxygen consumption with minimum lactate production (Goforth, 1990; Williams et al., 1993). However, the water being acted on by the flukes did not have a continuous flow velocity during these static experiments, and the force measured from the load cell could not be regarded as equivalent to the thrust generated during forward progression.

The thrust produced by dolphins from measurements based on bubble DPIV was found to be larger than the predicted viscous drag (Fig. 6). These results were in agreement with studies that used dynamic models of swimming (Webb, 1975; Chopra and Kambe, 1977; Yates, 1983; Fish, 1998a) rather than estimates of drag based on gliding or towing of rigid bodies. The magnitude of the viscous drag will depend on the wetted surface area of the body and flow conditions (laminar, turbulent, transitional) within the boundary layer (Webb, 1975; Skrovan et al., 1999). A boundary layer with turbulent flow produces higher viscous drag than a layer with a turbulent flow. The viscous drag on a flat plate with laminar boundary flow is considered the minimum resistive force. Recently, a numerical simulation showed that there is a very limited region of laminar flow and that the flow is mainly turbulent over the majority of the body of a dolphin swimming at  $3 \text{ m s}^{-1}$  (Riedeberger and Rist, 2012).

Numerous mechanisms were proposed to enable dolphins to maintain laminar boundary flow along their bodies and subsequently reduce total drag when swimming (see review by Fish and Hui, 1991). The assertion that the thrust generated by a swimming dolphin approaches or is equivalent to the drag of a rigid flat plate with a laminar boundary flow (Gray, 1936; Kramer, 1960a; Kramer, 1960b; Choi et al., 1997; Babenko and Carpenter, 2002; Romanenko, 2002; Nagamine et al., 2004) was not supported by bubble DPIV measurements (Fig. 5). The bottlenose dolphin has the ability to produce high thrust and power without requiring special drag-reducing mechanisms.

## MATERIALS AND METHODS

### Experimental animals

Experiments were conducted on two adult bottlenose dolphins (*T. truncatus*) (Table 2), which were maintained at the Long Marine Laboratory at the University of California, Santa Cruz. The dolphins were held in a large outdoor, marine pool (15.2×9.1×4.0 m), which was rectangular in shape with semi-circular ends. There were a number of underwater viewing windows (1.4×1.2 m), with four along one of the straight walls.

Dolphins were trained to swim at depth ( $\geq 1.5 \text{ m}$ ) through a sheet of microbubbles (see below). Experimental trials were divided into bouts of small amplitude swimming or large amplitude starts (Skrovan et al., 1999). For small amplitude swimming (i.e. vertical fluke displacement <20% of body length), the dolphin was trained either to swim on its own along the bubble sheet or to follow a target float at the end of a pole that was dragged underwater by a trainer. During these trials, the dolphin was already in motion as it passed the viewing window and was continually fluking (i.e. swimming by vertical oscillations of the caudal flukes). For large amplitude start trials, the dolphin was positioned in the bubble curtain within the field of view of the viewing window and held stationary by signal from the trainer. Under trainer command, the dolphin was released and initiated swimming by stroking its flukes with a large vertical displacement (i.e. fluke

displacement >20% of body length) that was greater than that observed for small amplitude swimming (Fish, 1993; Skrovan et al., 1999).

### Bubble DPIV

Microbubbles were generated from a compressed air source that was forced into a finely porous hose. The hose was located at the bottom of the pool approximately 2 m from the wall. The hose was held within a metal guide, which weighted the hose and kept it straight and parallel to the pool wall. Bubbles were initially less than 1 mm in diameter, though there was some coalescence as they rose to the surface. The size and density of the bubbles provided sufficient resolution for DPIV relative to the dimensions and swimming speed of the dolphins (Hart, 2000; Westerweel, 2000). The bubble sheet extended from the bottom of the pool to the surface with a length of 6.2 m and thickness of 2 cm. The bubble sheet was oriented along the dorso-ventral midline of the dolphin in the vertical ( $x, z$ ) plane. Natural sunlight was used to illuminate the microbubbles. There was a roughly 3-h period each day when sunlight could be used to optimally illuminate the bubble sheet for filming.

A Redlake MotionPro X3 high-speed video camera with a 28 mm, f1.4 lens (Vivitar, f2.5; Edison, NJ, USA) recorded the movements of the microbubbles as they were displaced by strokes of the flukes. The spatial resolution of the camera was  $1024 \times 1024$  pixels with a frame rate of 1000 full frames per second. The field of view was  $1 \times 1 \text{ m}$  and the fine interrogation windows were  $64 \times 64$  pixels. With  $4 \times$  oversampling, there were 64 vectors in each direction with a spacing between vectors of 1.56 cm in both the horizontal and vertical directions. The camera was controlled using a digital delay/pulse generator setup to capture bursts of three successive video frames 1 ms apart, every 10 ms by manually triggering the system. Sequences of vector fields were captured at 100 vector fields per second for each run, which accurately resolved the formation and evolution of the dolphin's tail vortex generated with every stroke. The mean rise velocity of the bubbles was determined by capturing video of the bubble sheet without dolphins and subtracted from every measurement.

The 2D velocity fields caused by the displacements of the microbubbles were computed with DPIV software. The in-house software used in this study is described in Hsu (Hsu, 2000) and Hsu et al. (Hsu et al., 2000). This is a technique in which tracer images, microbubbles in this case, are tracked from one video frame to the next using standard cross-correlation techniques. Flow velocity information was obtained with the aid of small, nominally square, interrogation windows in each image pair.

### Thrust and drag calculations

Oscillations of the dolphins' flukes, like an oscillating hydrofoil, produce strong trailing vortices with rotation determined by the direction of motion of the fluke (Weihs, 1972). By defining and integrating along a closed contour around the core of each vortex generated by the dolphin's tail, the circulation,  $\Gamma$ , which is proportional to the lift, was calculated using the formula:

$$\Gamma = \int \mathbf{V} \cdot d\mathbf{s}, \quad (1)$$

where  $\mathbf{V}$  is the velocity around the contour and  $d\mathbf{s}$  is the corresponding differential tangent vector on the contour. For these measurements, a non-zero value of  $\Gamma$  implies the existence of a thrust-producing vortex.

For ease of calculation, a square contour aligned with the coordinate directions was chosen to simplify the integration. The size of the contour was chosen to be small enough to capture the vortex core, i.e. excluding the outer region of the vortex where diffusion and dissipation of vorticity would yield a reduced vortex strength, yet large enough to ensure accurate integration. One can see in Fig. 2, where individual velocity vectors were assigned colors proportional to their vorticity, that the vorticity is highest in the center of the vortex and decreases outside of the vortex core. This region of maximum vorticity is noticeably smaller than the circular flow pattern, which is recognizable as the entire vortex. A sensitivity analysis of size and placement of the contour is provided in Legac (Legac, 2008).

Multiple separate runs were made using two different dolphins. A number of runs were discarded because the dolphin did not center itself on the bubble sheet. In a few cases, it was possible to capture multiple vortices generated from a number of tail oscillations. However, many of the runs produced only a single measurable vortex.

**Table 2. Morphometrics of dolphins (*Tursiops truncatus*) tested**

Dolphin	Sex	Length (m)	Mass (kg)	Fluke span (m)
Primo	Male	2.41	181.5	0.67
Puka	Male	2.46	205.5	0.68



For small amplitude swimming, thrust production was measured from the vortex strength through the two-dimensional airfoil Kutta–Joukowski theorem of aerodynamics. The thrust,  $T$ , is proportional to the circulation of the shed vortex,  $\Gamma$ , the vertical speed of the tail and the span of the tail, according to:

$$T = \rho \Gamma V_{\text{tail}} b, \quad (2)$$

where  $V_{\text{tail}}$  is the vertical velocity of the tail, perpendicular to the direction of swimming,  $\rho$  is the fluid density ( $1024 \text{ kg m}^{-3}$  for seawater) and  $b$  is the span of the dolphin's flukes.

In applying the Kutta–Joukowski theorem to this situation, it is important to note that the vortex shed by the dolphin is highly three-dimensional by virtue of the finite aspect ratio (AR) of the tail. Because the camera aperture and the width of the bubble column were the only way to restrict the depth of field, the DPIV measurements were necessarily spatially averaged across the span of the tail. As such, the computed circulation, and therefore the thrust, inherently contains a correction for the three-dimensionality of the tail; the circulation is by no means the idealized value that would be obtained using a two-dimensional fluke cross-section in a wind tunnel.

If one were to take the contrary perspective that the circulation measurement was, in fact, close to the two-dimensional ideal, one could apply a correction from Abbott and von Doenhoff (Abbott and von Doenhoff, 1959). Using the definition of AR as the square of the tail span,  $b$ , divided by the planform area of the tail,  $S$  (i.e.  $b^2/S$ ), there would be an ~20% reduction in thrust relative to the values shown in Fig. 4. This is based on the observation that the AR of an adult bottlenose dolphin tail is ~3.5. To see this, one can simplistically model one fluke to be a triangle with a span 1.5–2 times the base tail chord length. The AR is then between three and four. Based on data from Abbott and von Doenhoff (Abbott and von Doenhoff, 1959), this corresponds to an ~20% reduction in lift from the two-dimensional ideal case. For AR=1, lift is reduced by a factor of two. There would be a smaller reduction in thrust as the AR of the flukes of *Tursiops truncatus* ranges from 3.61 to 4.69 (Fish, 1993). But even if such a correction were appropriate, the conclusion that the thrust generated by a dolphin is more than large enough to overcome the drag would not change.

To see the relationship between thrust and tail motion, it is perhaps easiest to consider the case of a dolphin doing a tail stand. In that case, the oscillatory motion of the tail is analogous to a high angle of attack, finite wing moving back and forth horizontally in the water. With each transit, the tail (or wing) generates lift. This lift force, in turn, holds the dolphin up out of the water. The important thing to recognize is that the tail motion is perpendicular to the axis of the body, and that the 'lift' vector generated by the tail therefore points along the body axis toward the head. When the dolphin is swimming, then, the tail motion is vertical, and the 'lift' generated by the tail is oriented horizontally. As such, the formula in Eqn 1 is one and the same as the dolphin's thrust.

The thrust power output in watts was calculated as  $T$  times the swimming velocity of the dolphin. To avoid errors in momentum estimation due to the use of PIV, analysis was performed on sequences in which the vortex ring cross-sections were circular (Stamhuis and Nauwelaerts, 2005).

For small amplitude swimming, thrust is equal in magnitude and opposite in direction to drag (Webb, 1975; Vogel, 1994) so the drag coefficient,  $C_D$ , is:

$$C_D = T / 0.5\rho A V_{\text{swim}}^2, \quad (3)$$

where  $A$  is the wetted surface area of the body ( $\text{m}^2$ ) and  $V_{\text{swim}}$  is swimming speed ( $\text{m s}^{-1}$ ).  $A$  was calculated from eqn 1 of Fish (Fish, 1993), based on body mass. As the dolphins were not swimming near the water surface and at a submergence depth that was at least three times the body diameter, no correction was necessary because of increased drag due to surface wave formation (Hertel, 1966; Au and Weihs, 1980).

Comparisons of  $C_D$  with data from other studies and theoretical models was based on dimensionless Reynolds number ( $Re$ ).  $Re$  was computed from the dolphins' length ( $L$ , m),  $V_{\text{swim}}$  and the kinematic viscosity ( $\nu$ ) of seawater ( $1.044 \times 10^{-6} \text{ m}^2 \text{ s}^{-1}$ ) using the expression:

$$Re = LV_{\text{swim}} / \nu. \quad (4)$$

Variation about means was expressed as  $\pm 1$  s.d. All least-squares regressions and correlation coefficients were calculated using KaleidaGraph software (version 4.03, Synergy Software, Reading, PA, USA). Correlation coefficients were determined to be statistically significant at a level of  $P < 0.05$ .

#### Acknowledgements

We wish to express our appreciation to the training staff of the Long Marine Laboratory of the University of California, Santa Cruz, particularly Traci Kendall and Beau Richter. Support for the development of the full flow field measurement capability from the USA Swimming National Team (Russell Mark) is gratefully acknowledged.

#### Competing interests

The authors declare no competing financial interests.

#### Author contributions

F.E.F., T.M.W. and T.W. conceived and designed the experiments. F.E.F., P.L., T.M.W. and T.W. performed the experiments. F.E.F., P.L. and T.M.W. analyzed the data and designed the bubble DPIV method. F.E.F., T.M.W. and T.W. wrote the paper.

#### Funding

The research was supported in part by the Office of Naval Research (ONR) grant N00014-13-1-0808 to T.M.W.

#### References

- Abbott, I. H. and von Doenhoff, A. E. (1959). *Theory of Wing Sections*. New York, NY: Dover.
- Adrian, R. J. (1984). Scattering particle characteristics and their effect on pulsed laser measurements of fluid flow: speckle velocimetry vs particle image velocimetry. *Appl. Opt.* **23**, 1690–1691.
- Adrian, R. J. and Yao, C. S. (1985). Pulsed laser technique application to liquid and gaseous flows and the scattering power of seed materials. *Appl. Opt.* **24**, 44–52.
- Aleyev, Y. G. (1977). *Nekton*. The Hague: Junk.
- Aleyev, Y. G. and Kurbatov, B. V. (1974). Hydrodynamic drag of living fishes and some other nekton in the section of inertial movement. *Voprosy Ikhtologii* **14**, 173–176.
- Anderson, J. M., Streitlien, K., Barrett, D. S. and Triantafyllou, M. S. (1998). Oscillating foils of high propulsive efficiency. *J. Fluid Mech.* **360**, 41–72.
- Anderson, E. J., McGillis, W. R. and Grosenbaugh, M. A. (2001). The boundary layer of swimming fish. *J. Exp. Biol.* **204**, 81–102.
- Au, D. and Weihs, D. (1980). At high speeds dolphins save energy by leaping. *Nature* **284**, 548–550.
- Babenko, V. V. and Carpenter, P. W. (2002). Dolphin hydrodynamics. In *Flow Past Highly Compliant Boundaries and in the Collapsible Tubes* (ed. P. W. Carpenter and T. J. Pedley), pp. 31.1–13.31. London: Kluwer Academic Publishers.
- Borazjani, I. and Daghooghi, M. (2013). The fish tail motion forms an attached leading edge vortex. *Proc. Biol. Sci.* **280**, 20122071.
- Bose, N. (1995). Performance of chordwise flexible oscillating propulsors using a time-domain panel method. *Int. Shipbuilding Prog.* **42**, 281–294.
- Bose, N. and Lien, J. (1989). Propulsion of a fin whale (*Balaenoptera physalus*): why the fin whale is a fast swimmer. *Proc. R. Soc. B* **237**, 175–200.
- Choi, K.-S., Yang, X., Clayton, B. R., Glover, E. J., Atlar, M., Semenov, B. N. and Kulik, V. M. (1997). Turbulent drag reduction using compliant surfaces. *Proc. R. Soc. A* **453**, 2229–2240.
- Chopra, M. G. and Kambe, T. (1977). Hydrodynamics of lunate-tail swimming propulsion. Part 2. *J. Fluid Mech.* **79**, 49–69.
- Daniel, T. L. (1984). Unsteady aspects of aquatic locomotion. *Am. Zool.* **24**, 121–134.
- Daniel, T. L., Jordan, C. and Grunbaum, D. (1992). Hydromechanics of swimming. In *Mechanics of Animal Locomotion (Advances in Comparative and Environmental Physiology)*, pp. 17–49. Berlin; New York, NY: Springer-Verlag.
- Dearolf, J. L., McLellan, W. A., Dillaman, R. M., Frierson, D., Jr and Pabst, D. A. (2000). Precocial development of axial locomotor muscle in bottlenose dolphins (*Tursiops truncatus*). *J. Morphol.* **244**, 203–215.
- Denny, M. W. (1993). *Air and Water*. Princeton, NJ: Princeton University Press.
- Dong, P., Hsu, T. Y., Atsavaprane, P. and Wei, T. (2001). Digital particle image velocimetry. *Exp. Fluids* **30**, 626–632.
- Drucker, E. G. and Lauder, G. V. (1999). Locomotor forces on a swimming fish: three-dimensional vortex wake dynamics quantified using digital particle image velocimetry. *J. Exp. Biol.* **202**, 2393–2412.
- Drucker, E. G. and Lauder, G. V. (2001). Wake dynamics and fluid forces of turning maneuvers in sunfish. *J. Exp. Biol.* **204**, 431–442.
- Fish, F. E. (1993). Power output and propulsive efficiency of swimming bottlenose dolphins (*Tursiops truncatus*). *J. Exp. Biol.* **185**, 179–193.
- Fish, F. E. (1998a). Comparative kinematics and hydrodynamics of odontocete cetaceans: morphological and ecological correlates with swimming performance. *J. Exp. Biol.* **201**, 2867–2877.
- Fish, F. E. (1998b). Biomechanical perspective on the origin of cetacean flukes. In *The Emergence of Whales: Evolutionary Patterns in the Origin of Cetacea* (ed. J. G. M. Thewissen), pp. 303–324. New York, NY: Plenum Press.

- Fish, F. E. (2006). The myth and reality of Gray's paradox: implication of dolphin drag reduction for technology. *Bioinspir. Biomim.* **1**, R17-R25.
- Fish, F. E. and Hui, C. A. (1991). Dolphin swimming: a review. *Mammal Rev.* **21**, 181-196.
- Fish, F. E. and Lauder, G. V. (2006). Passive and active flow control by swimming fishes and mammals. *Annu. Rev. Fluid Mech.* **38**, 193-224.
- Fish, F. E. and Rohr, J. (1999). *Review of Dolphin Hydrodynamics and Swimming Performance (SSC Technical Report 1801)*. San Diego, CA: SPAWARS System Center.
- Fish, F. E., Innes, S. and Ronald, K. (1988). Kinematics and estimated thrust production of swimming harp and ringed seals. *J. Exp. Biol.* **137**, 157-173.
- Fish, F. E., Peacock, J. E. and Rohr, J. J. (2003). Stabilization mechanism in swimming odontocete cetaceans by phased movements. *Mar. Mamm. Sci.* **19**, 515-528.
- Fish, F. E., Nusbaum, M. K., Beneski, J. T. and Ketten, D. R. (2006). Passive cambering and flexible propulsors: cetacean flukes. *Bioinspir. Biomim.* **1**, S42-S48.
- Fish, F. E., Beneski, J. T. and Ketten, D. R. (2007). Examination of the three-dimensional geometry of cetacean flukes using CT-scans: hydrodynamic implications. *Anat. Rec.* **290**, 614-623.
- Flammang, B. E., Lauder, G. V., Troolin, D. R. and Strand, T. E. (2011). Volumetric imaging of fish locomotion. *Biol. Lett.* **7**, 695-698.
- Fontanella, J. E., Fish, F. E., Rybczynski, N., Nweeia, M. T. and Ketten, D. R. (2011). Three-dimensional geometry of the narwhal (*Monodon monoceros*) flukes in relation to hydrodynamics. *Mar. Mamm. Sci.* **27**, 889-898.
- Goforth, H. W. (1990). Ergometry (exercise testing) of the bottlenose dolphin. In *The Bottlenose Dolphin* (ed. S. Leatherwood), pp. 559-574. New York, NY: Academic Press.
- Gray, J. (1936). Studies in animal locomotion VI. The propulsive powers of the dolphin. *J. Exp. Biol.* **13**, 192-199.
- Grega, L. M., Wei, T., Leighton, R. I. and Neves, J. C. (1995). Turbulent mixed boundary flow in the corner formed by a solid wall and a free surface. *J. Fluid Mech.* **294**, 17-46.
- Hart, D. P. (2000). PIV error correction. *Exp. Fluids* **29**, 13-22.
- Hertel, H. (1966). *Structure, Form, Movement*. New York: Reinhold.
- Hsu, T. Y. (2000). *Turbulent Secondary Flow in the Mixed Boundary Corner Formed by a Horizontal Free Surface and a Vertical Solid Wall*. MSc thesis, Rutgers, The State University, New Brunswick, NJ, USA.
- Hsu, T. Y., Grega, L. M., Wei, T. and Leighton, R. I. (2000). Turbulent kinetic energy transport in a corner formed by a solid wall and a free surface. *J. Fluid Mech.* **410**, 343-366.
- Hui, C. (1987). Power and speed of swimming dolphins. *J. Mammal.* **68**, 126-132.
- Josephson, R. K. (1993). Contraction dynamics and power output of skeletal muscle. *Annu. Rev. Physiol.* **55**, 527-546.
- Katz, J. and Wehs, D. (1978). Hydrodynamic propulsion by large amplitude oscillation of an airfoil with chordwise flexibility. *J. Fluid Mech.* **88**, 485-497.
- Kayan, V. P. (1974). Resistance coefficient of the dolphin. *Bionika* **8**, 31-35.
- Kayan, V. P. (1979). The hydrodynamic characteristics of the caudal fin of the dolphin. *Bionika* **13**, 9-15.
- Kermack, K. A. (1948). The propulsive power of blue and fin whales. *J. Exp. Biol.* **25**, 237-240.
- Kramer, M. O. (1960a). Boundary layer stabilization by distributed damping. *J. Am. Soc. Naval Eng.* **72**, 25-34.
- Kramer, M. O. (1960b). The dolphins' secret. *New Sci.* **7**, 1118-1120.
- Lan, C. E. (1979). The unsteady quasi-vortex-lattice method with applications to animal propulsion. *J. Fluid Mech.* **93**, 747-765.
- Lang, T. G. (1966). Hydrodynamic analysis of cetacean performance. In *Whales, Dolphins and Porpoises* (ed. K. S. Norris), pp. 410-432. Berkeley, CA: University of California Press.
- Lang, T. G. (1975). Speed, power, and drag measurements of dolphins and porpoises. In *Swimming and Flying in Nature* (ed. T. Y. Wu, C. J. Brokaw and C. Brennen), pp. 553-571. New York, NY: Plenum Press.
- Lang, T. G. and Daybell, D. A. (1963). Porpoise performance tests in a seawater tank. In *NOTS TP 3063 (NAVWEPS Report 8060)*. China Lake, CA: Naval Ordnance Test Station.
- Lang, T. G. and Pryor, K. (1966). Hydrodynamic performance of porpoises (*Stenella attenuata*). *Science* **152**, 531-533.
- Lauder, G. V., Nauen, J. C. and Drucker, E. G. (2002). Experimental hydrodynamics and evolution: function of median fins in ray-finned fishes. *Integr. Comp. Biol.* **42**, 1009-1017.
- Legac, P. (2008). *Mechanics and Thrust Production of Mammalian Swimmers*. MSc thesis, Rensselaer Polytechnic Institute, Troy, NY, USA.
- Lighthill, J. (1969). Hydrodynamics of aquatic animal propulsion – a survey. *Annu. Rev. Fluid Mech.* **1**, 413-446.
- Lighthill, J. (1970). Aquatic animal propulsion of high hydromechanical efficiency. *J. Fluid Mech.* **44**, 265-301.
- Lighthill, J. (1971). Large-amplitude elongate-body theory of fish locomotion. *Proc. R. Soc. B* **179**, 125-138.
- Liu, P. and Bose, N. (1993). Propulsive performance of three naturally occurring oscillating propeller planforms. *Ocean Eng.* **20**, 57-75.
- Liu, P. and Bose, N. (1997). Propulsive performance from oscillating propulsors with spanwise flexibility. *Proc. R. Soc. A* **453**, 1763-1770.
- Liu, H., Wassersug, R. J. and Kawachi, K. (1997). The three-dimensional hydrodynamics of tadpole locomotion. *J. Exp. Biol.* **200**, 2807-2819.
- Müller, U. K., van den Heuvel, B. L. E., Stamhuis, E. J. and Videler, J. J. (1997). Fishfoot prints: morphology and energetics of the wake behind a continuously swimming mullet (*Chelon labrosus* Risso). *J. Exp. Biol.* **200**, 2893-2906.
- Nagai, M. (1999). *Thinking Fluid Dynamics with Dolphins*. Tokyo: IOS Press.
- Nagamine, H., Yamahata, K., Hagiwara, Y. and Matsubara, R. (2004). Turbulence modification by compliant skin and strata-corneas desquamation of a swimming dolphin. *J. Turbul.* **5**, N18.
- Norris, K. S. and Prescott, J. H. (1961). *Observations on Pacific Cetaceans of California and Mexican Waters*, pp. 291-401. Berkeley, CA: University of California Press.
- Parry, D. A. (1949). The swimming of whales and a discussion of Gray's paradox. *J. Exp. Biol.* **26**, 24-34, 2.
- Purves, P. E. (1969). The structure of the flukes in relation to laminar flow in cetaceans. *Z. Saugetierkd.* **34**, 1-8.
- Purves, P. E., Dudok van Heel, W. H. and Jonk, A. (1975). Locomotion in dolphins. Part I: Hydrodynamic experiments on a model of the bottle-nosed dolphin, *Tursiops truncatus*, (Mont.). *Aquatic Mammals* **3**, 5-31.
- Rayner, J. M. V. (1985). Vorticity and propulsion mechanics in swimming and flying animals. In *Konstruktionsprinzipien lebender und ausgestorbener Reptilien* (ed. J. Riess and E. Frey), pp. 89-118. Tübingen, FRG: University of Tübingen.
- Riedeberger, D. and Rist, U. (2012). Numerical simulation of laminar-turbulent transition on a dolphin using the  $\gamma$ -Re model. In *High Performance Computing in Science and Engineering '11* (ed. W. E. Nagel, D. B. Kröner and M. Resch), pp. 379-391. Berlin: Springer.
- Rohr, J. J. and Fish, F. E. (2004). Strouhal numbers and optimization of swimming by odontocete cetaceans. *J. Exp. Biol.* **207**, 1633-1642.
- Romanenko, E. V. (2002). *Fish and Dolphin Swimming*. Sofia: Pensoft.
- Schultz, W. W. and Webb, P. W. (2002). Power requirements of swimming: do new methods resolve old questions? *Integr. Comp. Biol.* **42**, 1018-1025.
- Sfakiotakis, M., Lane, D. M. and Davies, J. B. C. (1999). Review of fish swimming modes for aquatic locomotion. *IEEE J. Ocean. Eng.* **24**, 237-252.
- Skrovan, R. C., Williams, T. M., Berry, P. S., Moore, P. W. and Davis, R. W. (1999). The diving physiology of bottlenose dolphins (*Tursiops truncatus*). II. Biomechanics and changes in buoyancy at depth. *J. Exp. Biol.* **202**, 2749-2761.
- Stamhuis, E. J. and Nauwelaerts, S. (2005). Propulsive force calculations in swimming frogs. II. Application of a vortex ring model to DPIV data. *J. Exp. Biol.* **208**, 1445-1451.
- Triantafyllou, G. S. and Triantafyllou, M. S. (1995). An efficient swimming machine. *Sci. Am.* **272**, 64-70.
- Triantafyllou, G. S., Triantafyllou, M. S. and Gopalkrishnan, R. (1991). Wake mechanics for thrust generation in oscillating foils. *Phys. Fluids A* **3**, 2835-2837.
- Triantafyllou, G. S., Triantafyllou, M. S. and Grosenbaugh, M. A. (1993). Optimal thrust development in oscillating foils with application to fish propulsion. *J. Fluids Struct.* **7**, 205-224.
- Videler, J. and Kamermans, P. (1985). Differences between upstroke and downstroke in swimming dolphins. *J. Exp. Biol.* **119**, 265-274.
- Vogel, S. (1994). *Life in Moving Fluids*. Princeton, NJ: Princeton University Press.
- Webb, P. W. (1975). *Hydrodynamics and Energetics of Fish Propulsion*. Ottawa: Department of the Environment, Fisheries and Marine Service.
- Wehs, D. (1972). Semi-infinite vortex trails, and their relation to oscillating airfoils. *J. Fluid Mech.* **54**, 679-690.
- Weis-Fogh, T. and Alexander, R. MN. (1977). The sustained power output from striated muscle. In *Scale Effects in Animal Locomotion* (ed. T. J. Pedley), pp. 511-525. London: Academic Press.
- Westerweel, J. (2000). Theoretical analysis of the measurement precision in particle image velocimetry. *Exp. Fluids* **29** Suppl., S3-S12.
- Willert, C. E. and Gharib, M. (1991). Digital particle image velocimetry. *Exp. Fluids* **10**, 181-193.
- Williams, T. M. and Kooyman, G. L. (1985). Swimming performance and hydrodynamic characteristics of harbor seals *Phoca vitulina*. *Physiol. Zool.* **58**, 576-589.
- Williams, T. M., Friedl, W. A., Fong, M. L., Yamada, R. M., Sedivy, P. and Haun, J. E. (1992). Travel at low energetic cost by swimming and wave-riding bottlenose dolphins. *Nature* **355**, 821-823.
- Williams, T. M., Friedl, W. A. and Haun, J. (1993). Balancing power and speed in bottlenose dolphins (*Tursiops truncatus*). *Symp. Zool. Soc. Lond.* **66**, 383-394.
- Wu, T. Y. (1971a). Hydrodynamics of swimming propulsion. Part 1. Swimming of a two-dimensional flexible plate at variable forward speeds in an inviscid fluid. *J. Fluid Mech.* **46**, 337-355.
- Wu, T. Y. (1971b). Hydrodynamics of swimming propulsion. Part 2. Some optimum shape problems. *J. Fluid Mech.* **46**, 521-544.
- Yamaguchi, H. and Bose, N. (1994). Oscillating foils for marine propulsion. In *Proceedings of the Fourth International Offshore and Polar Engineering Conference*, pp. 539-544. Golden, CO: International Society of Offshore and Polar Engineers (ISOPE).
- Yates, G. T. (1983). Hydromechanics of body and caudal fin propulsion. In *Fish Biomechanics* (ed. P. W. Webb and D. Wehs), pp. 177-213. New York, NY: Praeger.
- Yazdi, P., Kilian, A. and Culik, B. M. (1999). Energy expenditure of swimming bottlenose dolphins (*Tursiops truncatus*). *Mar. Biol.* **134**, 601-607.